

NUMERICAL SIMULATION OF GAS-LIQUID FLOW IN GAS-AGITATED TANKS

Tao Song^{1,2}, Yuqing Feng¹, Junwu Zhou², Kaixi Jiang²

CSIRO Mathematics, Informatics and Statistics, Clayton VIC 3168, Australia
Beijing General Research Institute of Mining and Metallurgy, Beijing 100070, China

ABSTRACT

Gas-agitated reactors are widely used in the hydrometallurgical industry, including cyanide leaching of gold, uranium leaching, the bacterial oxidation of pyrite and copper leaching. To predict the performance of this kind of gas-agitated reactors, a numerical simulation method is presented for gas-liquid flow driven by bubbles. Gas-liquid flow is modelled using the Eulerian-Eulerian two-fluid equations, and extra user defined subroutines are incorporated to consider the complex physics, such as bubble induced turbulence and turbulent dispersion force. From the different interaction forces between gas and liquid, the turbulent dispersion force and drag force are particularly considered, because of their important impacts on bubble flow in gas-liquid system. The simulation results have been compared with the experimental measurements and numerical simulations of A. Sokolichin *et al.* (2004) and have given evidenced solutions. The simulations are also compared with the experiments of R. Shekhar and J.W. Evans (1989) for gas-liquid pattern and gas holdup in different operation and design parameters. In comparison with this data, reasonable agreements are obtained and the prediction of gas-liquid flow suggests that the model can be used to improve the performance of gas-agitated tanks.

NOMENCLATURE

C_d drag coefficient [dimensionless]
 C_k coefficient of bubble induced turbulence kinetic energy [dimensionless]
 C_e coefficient of bubble induced turbulence energy dispersion [dimensionless]
 C_μ k - ϵ turbulent model constant [dimensionless]
 d diameter [m]
 E_o Eotvos number [dimensionless]
 F drag force [N m^{-3}]
 g gravity vector [m s^{-2}]
 k turbulent kinetic energy [$\text{m}^2 \text{s}^{-2}$]
 p pressure [Pa]
 Pr Prandtl Number [dimensionless]
 r volume fraction [dimensionless]
 S source
 S_k additional source term in k -equation
 S_e additional source term in ϵ -equation
 t time [s]
 T^{turb} turbulent stress tensor [N m^{-2}]
 U velocity vector [m s^{-1}]

Greek letters

ϵ turbulent eddy dissipation [s^{-1}]
 ρ density [kg m^{-3}]
 μ effective viscosity [N s m^{-2}]
 σ surface tension [kg s^{-2}]

Subscripts

t turbulent
 α phase number
 c continuous phase number
 d dispersed phase number

INTRODUCTION

Gas-agitated reactor vessels are widely used in hydrometallurgical industry, such as gold leaching, uranium leaching, and the bacterial oxidation of pyrite. The performances of these tanks mostly depend on the suspension of mineral particles and mass transfer process, which control the kinetics of reactions and are intimately linked to the motion of the liquid that results from the injection of gas through the base (Rodriguez *et al.*, 2007). So bubble induced gas-liquid flow is the basis of these gas-agitated reactors and of the efficiency of metallurgical plants. For both economic and environmental reasons, modifications to device design are continuously being sought to reduce energy consumption and to increase productivity. A detailed understanding of bubble driven gas-liquid flow is critical to achieve these design improvements.

Following the advances of the computing speed and parallelisation technology, improved software solving algorithms, computational fluid dynamics (CFD) modelling can predict a lot of complex flow phenomena. Today, CFD models play an increasingly important role in process design, control and/or optimisation of process units in various process industries, e.g. mineral processing. The published literature implies that the predictive power of CFD simulations for bubble flow is already at a reliable level, since in most cases good agreements between experimental results and simulations have been shown. However, in modelling of gas-liquid flow, such as gas-liquid dispersion, there are still lots of additional complexities. The question of which physical effects are of prime importance and how they should be modelled is still under strong debate as there are no general formula and coefficient that can reliably describe all bubbly flow systems.

CSIRO has applied the coupled use of CFD and physical modelling to develop a bubble driven flow CFD model for aluminium smelting process. A time-averaged (steady state) bubble driven flow model has been developed and validated using a full scale air-water model of part of an aluminium reduction cell as a test-bed (Feng et al, 2010a, b). It was demonstrated that extra source terms were required to consider the bubble induced turbulence and bubble induced turbulent dispersion force. These terms are strongly case dependent. It is interesting to test whether the developed model can be applied to gas-stirred systems.

In this paper, a CFD model has been setup based on literature experimental geometry for model validation purpose. A 3D laboratory scale flat airlift loop reactor used in the experimental measurements and simulations of Sokolichin *et al.* (2004) is modelled first. The level of bubble induced turbulence is included based on the experimental work. Also, the role of turbulence dispersion force acting is assessed. The simulation results are compared with the original work and give a good agreement. The model is further extended to simulate a Pachuca gas-stirred tank where experimental data is available for comparison (Shekhar and Evans 1989).

MODEL DESCRIPTION

The governing equations are an extension of the continuity and Navier-Stokes equations for multiphase systems, essentially conservation equations for mass and momentum (Feng *et al.*, 2010). For gas-liquid system being studied here, the equations are averaged over the phase structure so as to give time-averaged equations for each phase (Lane *et al.*, 2005). As discussed in published literatures, the closely relevant forces which have important influences on the simulation results in the mathematical models are the pressure force, the drag force and the turbulent dispersion force. Another important factor is the bubble induced turbulence which has a strong influence on the mass diffusion and mixing.

Governing equations

The continuity equation and momentum equation take the following form (where $\alpha = c$ for liquid, $\alpha = d$ for gas):

$$\frac{\partial(r_\alpha \rho_\alpha)}{\partial t} + \nabla \cdot (r_\alpha \rho_\alpha U_\alpha) = 0 \quad (1)$$

$$\begin{aligned} \frac{\partial(r_\alpha \rho_\alpha U_\alpha)}{\partial t} + \nabla \cdot (r_\alpha (\rho_\alpha U_\alpha \otimes U_\alpha)) &= -r_\alpha \nabla p_\alpha \\ &+ \nabla \cdot r_\alpha T_\alpha^{turb} + S_{M_\alpha} + M_\alpha + r_\alpha \rho_\alpha g \end{aligned} \quad (2)$$

Here r_α is the phase volume fraction, ρ_α is the density, t is time, U_α is the mean velocity vector for each phase, and p_α is pressure. S_{M_α} describes momentum sources due to external body forces, e.g. buoyancy. M_α is the interfacial momentum transfer between phases and can include several types, such as drag force, lift force, virtual mass force, wall lubrication force, inter-phase turbulent dispersion force, etc.

By applying the eddy viscosity hypothesis, the Reynolds stresses can be linearly related to the mean velocity

gradients in a manner analogous to the relationship between the stress and strain tensors in laminar Newtonian flow, so the effective turbulent stress tensor T_α^{turb} can be written in the following form:

$$T_\alpha^{turb} = \mu_\alpha (\nabla U_\alpha + (\nabla U_\alpha)^T) \quad (3)$$

where μ_α is effective viscosity.

The effective viscosity is sum of the molecular and turbulent viscosities:

$$\mu_\alpha = \mu_0 + \mu_t \quad (4)$$

Phase dependent turbulence models have been used here: the dispersed phase zero equation model for the gas phase and k - ε two-equation model for the liquid phase. The turbulence eddy viscosity is calculated as:

$$\mu_{tc} = C_\mu \rho_c \frac{k_c^2}{\varepsilon_c} \quad (5)$$

for the liquid phase, and:

$$\mu_{td} = \frac{\rho_d \mu_{tc}}{\rho_c P_r} \quad (6)$$

for the gas phase.

The parameter P_r is the turbulent Prandtl number relating the dispersed phase kinematic eddy viscosity to the continuous phase kinematic eddy viscosity. C_μ is the k - ε turbulent model constant (default value is 0.09). k and ε are the turbulence kinetic energy and turbulence dissipation rate respectively. As is standard practice, the transport equations for k and ε are assumed to take a form similar to the single-phase transport equations:

$$\begin{aligned} \nabla \cdot \left(r_c (\rho_c U_c k_c) - \left(\mu + \frac{\mu_{tc}}{\sigma_k} \right) \nabla k_c \right) \\ = r_c (p_c - \rho_c \varepsilon_c) + S_k \end{aligned} \quad (7)$$

$$\begin{aligned} \nabla \cdot \left(r_c (\rho_c U_c \varepsilon_c) - \left(\mu + \frac{\mu_{tc}}{\sigma_\varepsilon} \right) \nabla \varepsilon_c \right) \\ = r_c \frac{\varepsilon_c}{k_c} (C_{\varepsilon 1} p_c - C_{\varepsilon 2} \rho_c \varepsilon_c) + S_\varepsilon \end{aligned} \quad (8)$$

where $C_{\varepsilon 1}$, $C_{\varepsilon 2}$, σ_k , σ_ε are turbulence model constants, default values being 1.44, 1.92, 1.0 and 1.3 respectively. p_c is the turbulence production due to viscous production. S_k and S_ε represent inter-phase transfer for k and ε respectively (Feng *et al.*, 2010).

Extra model input is required to represent the real physics, of which, two factors considered here are bubble induced turbulence and bubble turbulent dispersion force.

Bubble induced turbulence

Bubbles rising in the gas-agitated tank will produce increased turbulence of the liquid phase, known as bubble induced turbulence. Various models have been proposed

in the literature to account for this mechanism, with the two most widely accepted being modifying bubble induced turbulence eddy viscosity and adding a source of bubble induced turbulent kinetic energy. Bubble induced turbulence is very case dependent, which prevents a universal form for general use and is still an active area of research, as reviewed by Sokolichin *et al.* (2004). For the model with a modified turbulence kinetic energy equation, the following source terms have been added to the k and ε equations (Feng *et al.*, 2010):

$$S_k = C_k \rho_c r_c (1 - r_c) (U_c - U_d)^2 \quad (9)$$

$$S_\varepsilon = C_\varepsilon \frac{\varepsilon}{k} S_k \quad (10)$$

Here C_k and C_ε are the coefficients of bubble induced turbulence kinetic energy and energy dissipation respectively.

Bubble turbulent dispersion force

A turbulence dispersion force is proposed in the literature to account for the diffusion of bubbles due to the random influence of turbulent eddies in the liquid. The Favre averaged turbulence dispersion force model, an option in the ANSYS CFX14 Solver, has been used in this study. The form is given as:

$$M_c^{TD} = -M_d^{TD} = -C_{TD} C_{cd} \frac{\nu_{tc}}{\sigma_{tc}} \left(\frac{\nabla r_d}{r_d} - \frac{\nabla r_c}{r_c} \right) \quad (11)$$

Here, C_{cd} is the momentum transfer for the interphase drag force, and σ_{tc} is the turbulent Schmidt number for continuous phase volume fraction, currently set to be 0.9. C_{TD} is taken to be 1.

Drag force

Another important consideration in gas-liquid models has been the specification of drag force on the bubbles. This can be the most important factor for determining gas holdup and distribution, since in the absence of acceleration a balance between drag and buoyancy forces determines the bubble slip velocity. It is common to describe the drag force F_d in the following form:

$$F_d = -\frac{1}{2} C_d \rho_c \pi \frac{d_b^2}{4} |U_d - U_c| (U_c - U_d) \quad (12)$$

d_b denotes here the bubble diameter, and C_d is the drag coefficient. Several drag coefficient correlations are available for the two fluid bubble flow regime. Both Ishii Zuber and Grace correlations are commonly used. In this article, all simulations are set with the Ishii and Zuber model.

A commercial CFD code ANSYS CFX14 has been used to obtain a solution of the above equations, and subroutines are implemented to calculate the bubble induced turbulence and the drag force. A gas outlet boundary condition has been used on the top surface of the column through which gas leaves the tank at the rate it arrives from below (an option called “degassing condition” in CFX). Wall solid boundaries were set as no slip for water and free slip for air.

RESULTS AND DISCUSSION

The test case geometry, a locally aerated flat bubble column, is the same as the column used in the simulation work of Sokolichin *et al.* (2004). Figure 1 presents a test case of a flat airlift loop reactor with 2.0 m in height, 0.5 m in width, and 0.08 m in depth. A central inner wall (1.45 m height, 0.03 m width located 0.16 m above the bottom) separates the two main parts of the bubble column. The liquid height is 1.9 m. The gas is injected by a sparger located 0.15 m from the left-hand side of the reactor, and the gas flow rate equals 4 L/min. A whole 3D geometry was built, with a grid of 72,520 cells.

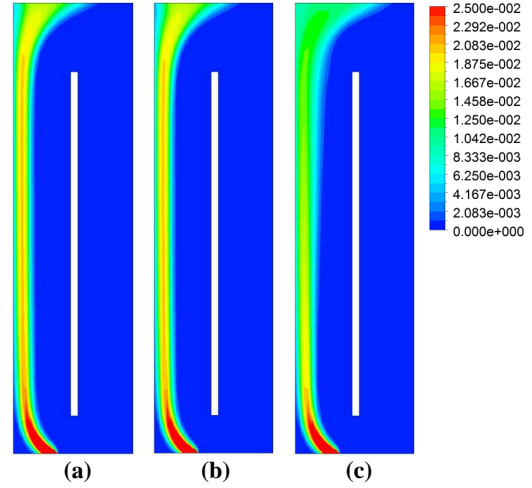


Figure 1: Flat column gas-agitated loop reactor under 4L/min gas flow rate. Simulation contour results of gas volume fraction at a centre plane of the column obtained. From left to right: (a) with standard CFX setup; (b) with the consideration of bubble induced turbulence; (c) with consideration of bubble induced turbulence and turbulent dispersion force.

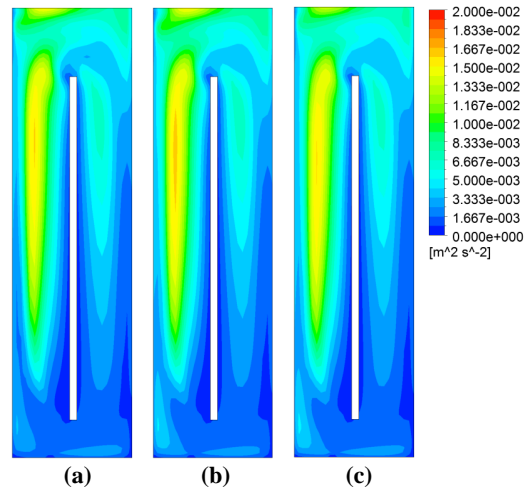


Figure 2: Flat column gas-agitated loop reactor under 4L/min gas flow rate. Simulation contour results of turbulent kinetic energy at a centre plane of the column obtained with standard $k-\varepsilon$ model. From left to right: (a) with standard CFX model; (b) with the consideration of bubble induced turbulence; (c) with consideration of bubble induced turbulence and turbulent dispersion force.

The simulation results with the same mesh information and boundary conditions are presented in Figure 1. With a standard setting from the CFX solver (e.g. without consideration of the bubble induced turbulence and turbulence dispersion force) a bubble plume has been generated, but the dispersion of the gas phase is underestimated, so that the gas bubbles accumulate exclusively near the left column wall (Figure 1a). Figure 2a shows the turbulence kinetic energy calculated based on the standard $k-\varepsilon$ equations. As expected, the turbulence level is higher at regions corresponding to high liquid velocities and gas volume fraction. However, the turbulence level is lower than the experimental measurement. This is because that the bubble induced turbulence is not considered. Following the suggested formula of Sokolichin *et al.* (2004), the bubble induced turbulence was included as an extra source term to the standard $k-\varepsilon$ equation. Thus, the turbulence level is increased a bit (Figure 2b), but there is little change on the bubble plume region (Figure 1b). From previous experience, the width of bubble plume region is sensitive to the bubble induced turbulent dispersion force. When this source term (Equation 11) is added on the momentum equation (2), the bubble plume area becomes wider (Figure 1c), which gives a better agreement with experimental observation. Interestingly, the maximum level of turbulence reduces (Figure 2c). This is because of the inter-related phenomena between gas volume fraction and bubble induced turbulence. Following the increase of bubble plume width, the maximum gas volume fraction reduces, thus, the bubble induced turbulence level reduces.

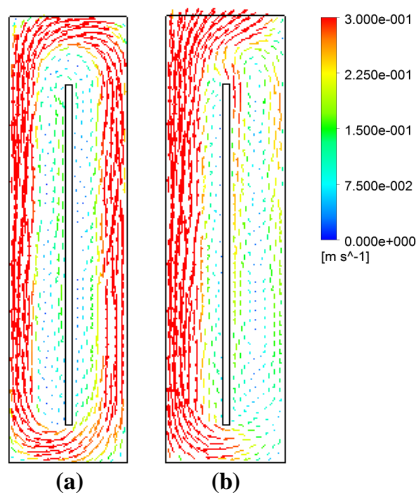


Figure 3: Flat column gas-agitated loop reactor under 4L/min gas flow rate. Simulation results obtained with standard $k-\varepsilon$ model, drag force, turbulent dispersion force and bubble induced turbulence in the mid-depth plane (a) liquid velocity, and (b) gas velocity.

In the test case, the application of bubble induced turbulence source term with adapted values of $C_k = 0.83$ and $C_\varepsilon = 0.13$ results in a much better agreement with the experimental result. Figure 3 shows the flow patterns for gas phase and liquid phase of the model with the consideration of bubble induced turbulence dispersion force and bubble induced turbulence. The good circulation flow of liquid phase near column wall has been generated by the injected gas flow at the bottom of the tank, which is

very close to the real flow field measured by LDA in experiments. Since the degassing boundary condition used here set a closed flow area for the liquid phase, the gas-liquid surface fluctuation was not simulated here. There are some small bubbles distributed in downcomer side of the column, which are brought by the high speed liquid flow. Although this phenomenon cannot be observed from the simulated gas holdup distribution (Figure 1c), the gas velocity field still shows a small circulation in the area where there could represent small bubbles (Figure 3b). The results qualitatively agree well with the experimental measurement. To give a quantitative validation of the current model, point-wise comparison between experimental data and the simulation data is required, which represent our on-going work.

The optimal parameter values, determined by fitting of experimental data, are strongly different from case to case. If the gas flow in the example of Figure 3 is reduced from 4 L/min to 2 L/min, the optimal values for C_k and C_ε change to be 1.2 and 2.0. Because of the lower gas flow rate, the bubble driven liquid recirculation reduces considerably (Figure 4a). Similarly, the turbulence level reduces (Figure 4c). It is interesting to see that the bubble plume area increases (Figure 4d). On the one hand, the level of turbulence reduces, the plume area would reduce. On the other hand, the reduction of liquid velocity leads to less push of the bubbles towards the left wall. The combined effect leads to a wider bubble plume area.

Another test simulation was made for gas-liquid flow in a laboratory-scale Pachuca tank, which was from Shekhar and Evans (1989). The Pachuca tank was 1.5 m high, 0.61 m in diameter and had a conical bottom (height = 0.3 m and cone half angle = 45 degree). The filled height was 1.21 m. The draft tube bottom (draft tube height = 0.91 m and draft tube diameter = 0.15 m) was positioned 0.23 m above the apex of the cone. Gas was injected into the tank through a single nozzle (diameter = 0.07 m) placed 0.025 m below the draft tube bottom at a gas superficial velocity of 0.0014 m/s. The geometry has been represented by a 10 degree section of the Pachuca tank, with a grid of 23,443 cells.

The industry experience and laboratory experiment knowledge present a secondary recirculation loop in the top half of the tank and a nearly stagnant region in the bottom half of the tank. In addition, in gas-stirred tanks, it is expected that agitation of the liquid will be lowest at the bottom and will increase greatly upon approaching the fluid surface because of the rapid expansion of gas bubbles near the surface (Shekhar, 1985).

The simulation results are shown in Figure 5 in terms of liquid flow field (Figure 5a), gas flow field (Figure 5b), turbulent kinetic energy distribution (Figure 5c) and gas volume fraction (Figure 5d) in the mid-depth plane. Top circulation loop and bottom low speed stagnant region are clearly shown in the liquid flow field and gas flow field, which are consistent with the experimental observation. Turbulent kinetic energy k is in a high value at the top of the tank, but approximately two orders of magnitude lower in a zone extending from the top of the conical section to approximately halfway up the tank. This is also a region with low velocities, as can be seen from the gas flow field.

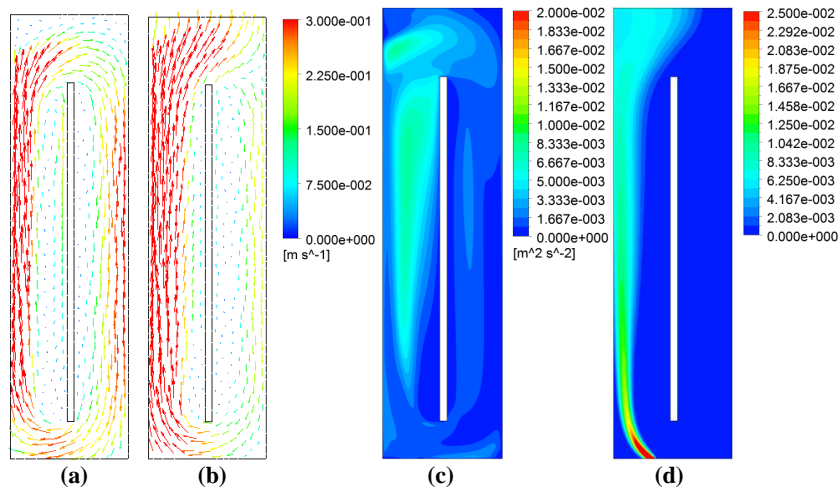


Figure 4: Flat column gas-agitated loop reactor under 2L/min gas flow rate. Simulation results obtained with standard $k-\epsilon$ model, drag force, turbulent dispersion force and bubble induced turbulence in the mid-depth plane. From left to right: (a) liquid velocity vector; (b) gas velocity vector; (c) turbulent kinetic energy; (d) gas volume fraction.

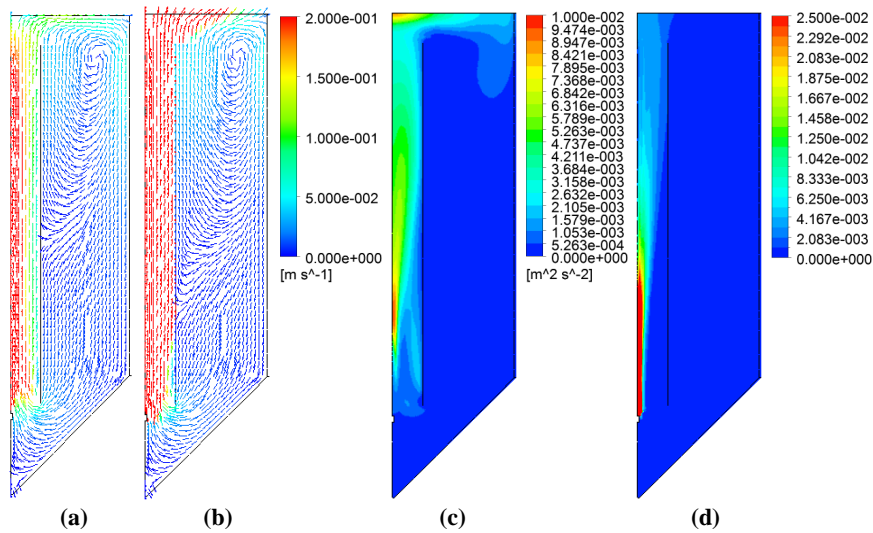


Figure 5: Pachuca tank under 0.0014 m/s gas superficial velocity. Simulation results obtained with standard $k-\epsilon$ model, drag force, turbulent dispersion force and bubble induced turbulence in the mid-depth plane. From left to right: (a) liquid velocity vector; (b) gas velocity vector; (c) turbulent kinetic energy; (d) gas volume fraction.

Figure 6 is the comparison of axial water velocity between simulation and experimental results under 0.0014 m/s gas superficial velocity. It can be seen that the simulation results are very close to the laboratory tests (Shekhar, 1989) in different depths of the tank, except the position near tank wall.

The simulation results indicate there are potentials to further improve the current design and/or operation. For example, the height of inside tube should be smaller (from 0.55 m to 0.8 m and the filled height keeps the same), then a better dispersion of gas phase can be achieved and the edge of the circulation loop is closer to tank and tube walls. A higher gas flow rate (gas superficial velocity = 0.0028 m/s) can bring a bigger bubble plume and better circulation.

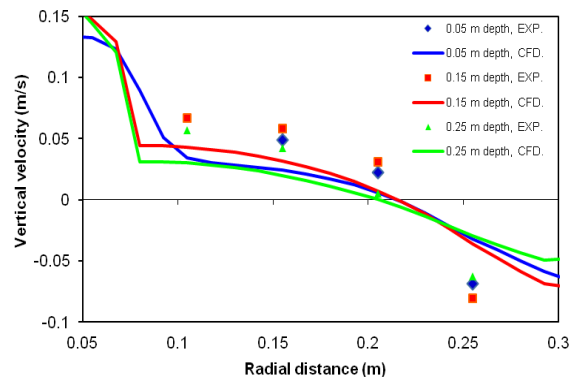


Figure 6: Comparison of axial water velocity between simulation and experiment when the gas superficial velocity is 0.0014 m/s.

CONCLUSION

The bubble driven liquid flow CFD model, developed for aluminium smelting process, has been extended to study two gas-stirred systems. With a proper consideration of the bubble induced turbulence and the turbulent dispersion force, the key flow patterns in a laboratory airlift reactor (Sokolichin *et al.*, 2004) and a Pachuca tank (Shekhar and Evans, 1989) can be predicted reasonably well.

The initial test demonstrated the usefulness of the developed model for capturing the complex flow structure, hence for a better understanding of the process, and eventually for further improvement of a specific design and/or operations. It also demonstrated that the flow is complex and the model input parameters are strongly case dependent, where detailed physical modelling data is required to justify the modelling input parameters quantitatively. To build a general constitutive correlation for gas liquid complex flow challenges the scientific community. This represents our on-going effort through combined use of advanced physical modelling and CFD modelling.

REFERENCES

- FENG, Y.Q., YANG, W., COOKSEY, M. and SCHWARZ, M.P., (2010a), "Development of Bubble Driven Flow CFD Model Applied for Aluminium Smelting Cells", *The Journal of Computational Multiphase Flows*, Volume 2, Number 3, 179-188.
- FENG, Y.Q., COOKSEY, M.A. and SCHWARZ, M.P., (2010b) "CFD modelling of alumina mixing in aluminium reduction cells", *Light Metals*, Seattle, WA, 455-460.
- LANE, G.L., SCHWARZ, M.P. and EVANS, G.M., (2005), "Numerical modelling of gas-liquid flow in stirred tanks", *Chemical Engineering Science*, 60, 2203-2214.
- RODRIGUEZ M., E., CASTILLEJOS E., A.H. and ACOSTA G., F.A., (2007), "Experimental and Numerical Investigation of Fluid Flow and Mixing in Pachuca Tanks", *Metallurgical and Materials Transactions B, Process Metallurgy and Materials Processing Science*, Volume 38, Issue 4, 641-656.
- SOKOLICHIN, A., EIGENBERGER, G. and LAPIN, A., (2004), "Simulation of buoyancy driven bubbly flow: established simplifications and open questions", *AIChE Journal*, 50, 2004, 24-44.
- SHEKHAR, R. and EVANS, J.W., (1989), "Fluid flow in Pachuca (Air-Agitated) Tanks: Part I. Laboratory-Scale Experimental Measurements", *Metallurgical Transactions B*, Volume 20B, 781-791.
- SHEKHAR, R., *M.S. Thesis*, University of California, Berkeley, 1985.
- ANSYS CFX-Solver Theory Guide*, (2011), ANSYS Inc.